SUPPLEMENTARY NOTES
Making it Stick: Convection, Reaction, and Diffusion in Surface-Based Biosensors

Todd M. Squires and Robert J. Messinger
Department of Chemical Engineering, University of California, Santa Barbara, CA 93106 USA

Scott R. Manalis
Departments of Biological and Mechanical Engineering,
Massachusetts Institute of Technology, Cambridge, MA 02139 USA
(Dated: February 6, 2008)

I. THEORY AND MODELING

A. Governing Equations

The equations of motion for an incompressible Newtonian fluid are

$$\rho(\frac{\partial \vec{u'}}{\partial t'} + \vec{u'} \cdot \nabla \vec{u'}) = -\nabla p' + \mu \nabla^2 \vec{u'} \quad (1)$$

$$\nabla \cdot \vec{u'} = 0 \quad (2)$$

where t' is time, ρ is the local fluid density, $\vec{u'}$ is the local fluid velocity, p' is the local pressure within in the fluid. Here, a prime denotes that a variable possesses dimensionality; the absence of a prime will indicate that a variable is dimensionless. The first equation is the Navier-Stokes equation, which is a continuum expression for the conservation of fluid momentum. The second equation is a continuum expression for the conservation of mass for an incompressible fluid. These equations must be solved simultaneously to calculate the velocity and pressure fields.

We model a 2-dimensional cross section of the channel for the simulations. The 2-D model assumes that wall effects that alter the velocity field in the width direction are negligible; this assumption is valid when $W_c \gg H$. Unidirectional pressure-driven flow through a 2-D channel has a parabolic velocity profile

$$\vec{u'}(y') = \frac{G}{2\mu} y'(H - y')\vec{e_x}, \quad (3)$$

where G is the axial pressure gradient, H is the channel height, and $\vec{e_x}$ is the unit normal vector in the x-direction. The volumetric flow rate per unit width is found by integrating the velocity field across the channel height to yield

$$Q/W_c = \int_0^H \vec{u}(y)dy = GH^3/12\mu. \quad (4)$$

which can be inserted into the velocity field expression, equation (3), to obtain

$$\vec{u'}(y') = \frac{6Q}{W_c H^3} y'(H - y')\vec{e_x}. \quad (5)$$

Concentration of a species that diffuses and is advected by a fluid flow obeys the partial differential equation

$$\frac{\partial c'}{\partial t'} = D\nabla'^2 c' - \vec{u'} \cdot \nabla c' + R, \quad (6)$$

the conservation equation for analyte with concentration c' and diffusivity D in a fluid flowing with velocity $\vec{u'}$ and bulk reaction rate R. In our system, $R = 0$ since the reaction only occurs at the sensor surface. The left-hand side represents local concentration changes and the right-hand side represents transport due to diffusion and convection.

We assume that the chemical kinetics can be described via the Langmuir binding model

$$\frac{\partial b'}{\partial t'} = k_{on} c'|_{y=0}(b_{max} - b') - k_{off} b', \quad (7)$$

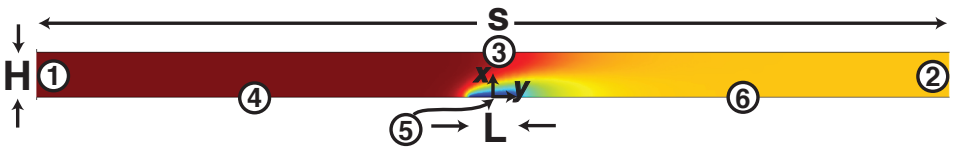

Supplementary Figure 1: Model system with labeled boundaries. The origin of the coordinate system is placed at the center of the sensor.

where k_{on} is the binding constant, k_{off} is the disassociation constant, b' is the surface concentration of bound analyte, and $b_{\max}$ is the density of binding sites on the sensor.

To solve for the analyte concentration field, equations (6) and (7) must be solved simultaneously. We have solved for the velocity field (equation 5), which can be inserted directly into equation (6); for more complicated geometries one would solve for the fluid velocity numerically.

The 2-D model system is depicted in Supplementary Figure 1. Defining the length of the channel as s (whose specific length must be chosen carefully, as discussed in section C), we define six boundaries as

$$\text{surface (1)} \;\rightarrow\; 0 \le y' \le H,\; x' = -s/2 \tag{8}$$
$$\text{surface (2)} \;\rightarrow\; 0 \le y' \le H,\; x' = s/2 \tag{9}$$
$$\text{surface (3)} \;\rightarrow\; -s/2 \le x' \le s/2,\; y' = H \tag{10}$$
$$\text{surface (4)} \;\rightarrow\; -L/2 \le x' \le L/2,\; y' = 0 \tag{11}$$
$$\text{surface (5)} \;\rightarrow\; 0 \le y' \le H,\; x' = s/2 \tag{12}$$
$$\text{surface (6)} \;\rightarrow\; L/2 \le x' \le s/2,\; y' = 0. \tag{13}$$

Defining $\vec{n}$ as the unit normal vector directed out of a surface, the boundary conditions to be satisfied on each boundary are given by:

$$c' = c_0 \quad \text{at} \quad \text{surface (1)} \tag{14}$$
$$\vec{n} \cdot D\nabla' c' = 0 \quad \text{at} \quad \text{surfaces (2), (3), (4), (6)} \tag{15}$$
$$\frac{\partial b'}{\partial t'} = -D\frac{\partial c'}{\partial y'} \quad \text{at} \quad \text{surface (4).} \tag{16}$$

Boundary condition (14) ensures that the solution entering the system has concentration c_0. Boundary conditions (15) ensure no analyte diffuses out through solid walls. The reaction/flux boundary condition (16) dictates the binding kinetics at the sensor surface. Assuming (first-order) Langmuir binding kinetics, eq. (16) is given by

$$\frac{\partial c'}{\partial y'} = -\frac{1}{D}[k_{\text{on}} c'|_{y'=0}(b_{\max} - b') - k_{\text{off}} b']. \tag{17}$$

B. Non-Dimensionalization of Governing Equations

By using appropriate scales for the system variables to non-dimensionalize the governing equations, we obtain *dimensionless* groups of parameters that characterize the important physics of the system. These dimensionless ratios typically represent competing processes (e.g. the Peclet number is the ratio of diffusive to convective flux, the Reynolds number is the ratio of inertial to viscous forces, and so on). These ratios can often be determined for a system without detailed computations, and their values (unity, very large, very small, etc.) typically give crucial intuition about how a system will behave. Non-dimensionalization also allows one to generate universal plots that can collapse relationships spanning orders of magnitude onto a single master curve. An example of this phenomenon is the plot of τ_R/τ_{CRD} vs. Da (Fig. 4) in the main article. Finally, non-dimensionalization allows the results of various numerical simulations and experiments to be compared in a truly meaningful fashion. Most undergraduate and graduate textboods on fluid mechanics will discuss dimensional analysis and non-dimensionalization. Below, the five dimensionless parameters in the main article (Pe_{H}, λ, Da, $\tilde{c}$, and ϵ) will emerge naturally via non-dimensionalization.

First, we non-dimensionalize the convection-diffusion equation (eq. 6) governing mass transport in the fluid, scaling concentration by input concentration ($c = c'/c_0$), axial distance by the sensor length ($x = x'/L$), transverse distances

by the channel height ($y = y'/H$), and time by diffusion time for analyte to traverse the channel ($t = D\ t'/H^2$). Equation (6) then becomes

$$\frac{\partial c}{\partial t} = \lambda^2 \frac{\partial^2 c}{\partial x^2} + \frac{\partial^2 c}{\partial y^2} - 6\lambda \mathrm{Pe_H}\ y(1-y)\frac{\partial c}{\partial x}, \tag{18}$$

where the dimensionless parameters $\mathrm{Pe_H} = Q/W_c D$ and $\lambda = H/L$ discussed in the main text have naturally emerged. Note that the diffusive terms are now *anisotropic* (λ^2 multiplies $\frac{\partial^2 c}{\partial x^2}$ term but not $\frac{\partial^2 c}{\partial y^2}$); this occurs because we have scaled axial and transverse distances differently in order to create a computational domain where the sensor length and channel height both have the same length, such that concentration fields around each can be resolved naturally. In some cases, it is numerically advantageous to choose different scalings, as discussed below.

Next, we non-dimensionalize the sensor binding kinetics (eq. 7). We scale the surface concentration of bound analyte by the binding site density ($b = b'/b_{\max}$) and time and concentration as above, yielding

$$\frac{\partial b}{\partial t} = \epsilon^*\ \mathrm{Da}^* \left(c_{y=0}(1-b) - \frac{1}{\tilde{c}} \right), \tag{19}$$

where

$$\epsilon^* = \frac{c_0 H}{b_{\max}}, \tag{20}$$

$$\mathrm{Da}^* = \frac{k_{\mathrm{on}} c_0 H}{D}, \tag{21}$$

$$\tilde{c} = \frac{k_{\mathrm{on}} c_0}{k_{\mathrm{off}}} = \frac{c_0}{K_D}. \tag{22}$$

The dimensionless parameters ϵ^*, Da^*, and $\tilde{c}$ arise simply from non-dimensionalizing the Langmuir binding kinetic equation. Note, however, that two of them (Da^* and ϵ^*) are defined differently than in the main text (where, *e.g.*, $\mathrm{Da} = k_{\mathrm{on}} b_{\max} \delta / D$). In both cases, the Damkohler number represents a ratio of reactive flux to diffusive flux. The diffusive flux depends upon the distance over which analyte must diffuse, which is not known *a priori*. In the text, we used physical intuition and scaling arguments to estimate this length δ, whereas for general numerical simulations, we choose a standard length scale (here H) based on the geometry of the system. Simulations for systems with different conditions are then performed by simply changing the dimensionless parameters as appropriate.

Equations (18) and (19) are dimensionless differential equations that govern the analyte concentration field and surface reaction kinetics, respectively. In the simulations, it is these two equations that are solved simultaneously via numerical finite-element methods. However, the boundary conditions (eqs. 14-16) must also be non-dimensionalized. Using the same scalings as above, we obtain

$$c = 1 \quad \text{at} \quad \text{surface (1)} \tag{23}$$

$$\vec{n} \cdot \nabla c = 0 \quad \text{at} \quad \text{surfaces (2), (3), (4), (6)} \tag{24}$$

$$\frac{\partial b}{\partial t} = -\epsilon^* \frac{\partial c}{\partial y} \quad \text{at} \quad \text{surface (4)}, \tag{25}$$

with surface locations non-dimensionalized to yield

$$\text{surface (1)} \ \rightarrow\ 0 \le y \le 1,\ x = -s/2L \tag{26}$$

$$\text{surface (2)} \ \rightarrow\ 0 \le y \le 1,\ x = s/2L \tag{27}$$

$$\text{surface (3)} \ \rightarrow\ -s/2L \le x \le s/2L,\ y = 1 \tag{28}$$

$$\text{surface (4)} \ \rightarrow\ -1/2 \le x \le 1/2,\ y = 0 \tag{29}$$

$$\text{surface (5)} \ \rightarrow\ 0 \le y \le 1,\ x = s/2L \tag{30}$$

$$\text{surface (6)} \ \rightarrow\ L/2 \le x \le s/2L,\ y = 0. \tag{31}$$

Using eq. (19), the reaction/flux boundary condition on the sensor becomes

$$\left.\frac{\partial c}{\partial y}\right|_{|x|<1/2, y=0} = -\mathrm{Da}^* \left(\left. c \right|_{y=0} (1-b) - \frac{1}{\tilde{c}} b \right). \tag{32}$$

C. Approaches and Considerations during Finite Element Simulations

For the main article, we performed simulations for three scenarios: (i) pure diffusion, (ii) convection and diffusion, and (iii) convection, reaction, and diffusion. Each case requires the (dimensionless) governing equations and boundary conditions to be modified, each differs in implementation and poses distinct computational challenges. Furthermore, microsensors and nanosensors place different demands upon the simulation geometry, and will also be discussed.

We wrote MATLAB code that employ COMSOL finite-element algorithms to define the geometry, initialize and refine the computational mesh, and numerically solve the governing equations subject to the boundary and/or initial conditions. For all simulations, we computed the dimensionless diffusive flux $\mathcal{F}$ numerically via

$$\mathcal{F} = \int_{-L/2}^{L/2} -\frac{\partial c}{\partial y} dx \tag{33}$$

1. Pure diffusion

This scenario involves the simulation of a sensor in a quiescent fluid with no kinetic limitations. The governing equation (6), is simplified by taking $\mathrm{Pe_H} = 0$ (so that the flow rate Q vanishes), to leave pure diffusion. These simulations are inherently transient, necessitating an initial condition, here taken to be simply $c = 1$ everywhere in the quiescent fluid.

We modify the boundary conditions as well – all no-flux boundaries remain so. Additionally, the condition at the inlet was changed to 'no diffusive flux' boundary condition $\vec{n} \cdot \nabla c = 0$, and the simulation geometry was chosen to ensure the diffusion zone did not reach the inlet and outlet boundaries. Finally, the reactive/flux boundary was taken to be a perfect collector ($c = 0$). This change imposes an infinitely fast reactive flux relative to the diffusive flux and an infinite binding site density; mathematically this is equivalent to letting $\mathrm{Da} \to \infty$ and $b_{max} \to \infty$.

Since no convection is present, this system is *never* reaches steady-state and the depletion region grows indefinitely as time evolves. To ensure that our 'artifical' simulation boundaries do not influence the results of the simulation, we choose the dimensionless channel length s/L such that the depletion zone never reaches the end of the channels over the timescale of the simulations. We can state this mathematically by imposing the condition $s/2L \gg \sqrt{\lambda^2 t_{\mathrm{final}}}$ where λ^2 is the effective x-diffusion coefficient and t_{final} is the final simulation time.

2. Convection and Diffusion

Here, we continue to treat the sensor as an ideal, perfect collector, so that rather than a kinetic reactive flux at the sensor surface, we impose perfect collection ($c = 0$); here, unlike in the pure diffusion case, we use a non-zero Pe_H.

The convection-diffusion system is simulated at steady-state. As above, the channel length s/L must be chosen such that the depletion region does not reach the entrance boundary. In the main text, we estimated the upstream distance the depletion zone extends to scale like $H/\mathrm{Pe_H}$. We thus require that the upstream distance $s/2L \gg 1/(\lambda\ \mathrm{Pe_H})$, assuming the sensor is located at the center of the computational domain. We can save computational effort, however, by shortening the length of the *downstream* channel that we simulate. If we shift the center of the sensor a distance Δx from the origin where $\Delta x < s/2L$, we obtain $(s/2L + \Delta x) \gg 1/(\lambda\ \mathrm{Pe_H})$. Typically, the sensor was shifted by a Δx such that any transverse downstream concentration gradients are still contained in the system.

An additional complication arises once convective transport is introduced: at high $\mathrm{Pe_H}$, thin boundary layers form, yielding gradients that occur over distances that are much shorter than one would naively estimate from geometry. As such, we must ensure that the computational mesh employed by the finite-element solver is fine enough to resolve the boundary layer. We therefore use different codes to simulate high and low $\mathrm{Pe_H}$ systems. Low-$\mathrm{Pe_H}$ systems are treated as above; high-$\mathrm{Pe_H}$ systems, on the other hand, require computational meshes that are highly refined near the sensor to sufficiently resolve these gradients. In these situations the mesh is locally initialized over the sensor with an exponential decay algorithm. The regions directly over the sensor then have a high density mesh and the regions far away from the sensor have a low density mesh. By doing so, all meshes are sufficiently dense to resolve local analyte concentration gradients, while avoiding unnecessary computational expenses.

In this steady state, we are interested in the fraction of the analyte molecules in solution that is collected by the sensor, and the fraction that is 'lost' upon flowing past the sensor. We define the 'retention' (collected fraction) R as

$$R = (\mathrm{J_{in}} - \mathrm{J_{out}})/\mathrm{J_{in}}, \tag{34}$$

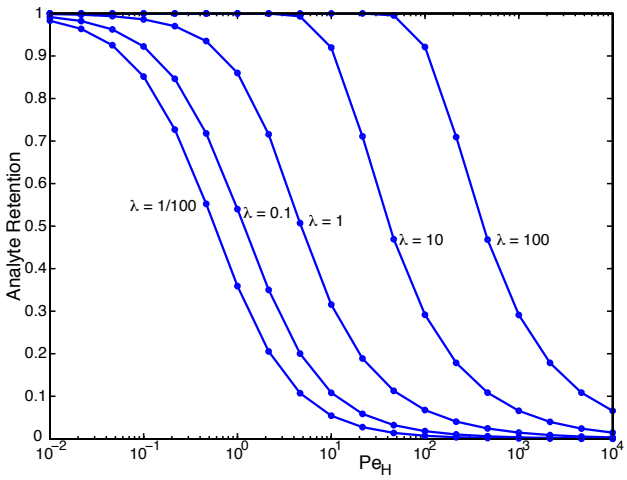

Supplementary Figure 2: Analyte Retention R vs. $\mathrm{Pe_H}$ at various values of λ for the convection and diffusion scenario.

where

$$J_{\mathrm{in}} = \int_0^H u_x(y)\; c|_{x=-s/2L}(y)dy, \tag{35}$$

and

$$J_{\mathrm{out}} = \int_0^H u_x(y)\; c|_{x=s/2L}(y)dy. \tag{36}$$

In other words, the retention R is the fraction of the incoming analyte flux that is collected. We plot the steady-state analyte retention R vs. $\mathrm{Pe_H}$ for various sensor sizes λ in Supplementary Figure 2.

3. Convection, Diffusion, and Reaction

Finally, the full convection-diffusion-reaction system involves the full system of equations presented above. These simulations are inherently transient and an initial condition $c = 1$ is specified to solve the governing equations. As with the convection and diffusion scenario above, we design the computational grid such that $s/L \gg 1/(\lambda\ \mathrm{Pe_H})$. The computational grid is chosen according to the (estimated) mass transport regime: we employ a highly-refined mesh near the sensor for high-$\mathrm{Pe_H}$ systems, for example. An additional complication that arises in solving this set of equations is that the sensor boundary condition itself involves an ordinary differential equation. We solve the convection-diffusion equation for mass transport in the bulk in weak form, and the boundary condition is integrated as an ODE, and two-way coupling between the boundary and the concentration field is enforced through COMSOL.

In the convection, reaction, and diffusion scenario, $\mathrm{Da} \gg 1$ indicates that the system is diffusion-limited and $\mathrm{Da} \ll 1$ indicates that the system is reaction-limited. If the system is reaction limited, then mass transport plays little role, and the concentration above the sensor, $c|_{(y=0}$, is very nearly equal to the bulk concentration c_0 in the Langmuir binding model. The Langmuir binding equation can then be solved analytically (equation (10) in the main article), giving a bound concentration that approaches equilibrium exponentially. A diffusion-limited system, on the other hand, has $c|_{y=0} \approx 0$, giving a diffusive flux that is nearly constant and a bound concentraiton $b(t)$ that grows approximately linearly in time. We plot the (scaled) bound concentration $b^\dagger = b'/b_{\mathrm{eq}}$ against (scaled) time $t^* = t'/\tau_{\mathrm{CRD}}$ in Supplementary Figure 3, for two different values of Da. WIth these scales, the sensor equilibrates at $b^* = 1$ and reaches $1 - 1/e = 0.63$ capacity at time $t^* = 1$. As expected, the diffusion-limited system has a bound concentration that grows linearly (slope ~ 1) and the reaction-limited bound concentration grows exponentially.

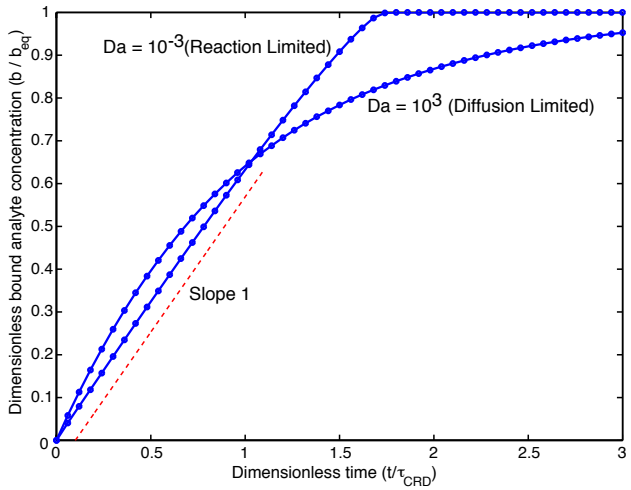

Supplementary Figure 3: Dimensionless analyte concentration vs. dimensionless time for a reaction-limited system ($\mathrm{Da} \ll 1$) and a diffusion-limited system ($\mathrm{Da} \gg 1$).

4. Microsensor and Nanosensor Simulations

The above strategies are effective, roughly speaking, for sensors that are approximately the same size as the channel height. Systems with $\lambda \ll 1$, as would occur for *e.g.* nanosensors, would be computationally quite difficult to resolve directly with extremely low aspect ratios. We thus describe our strategies for the worked examples (micro-sensor and nano-sensor).

We simulate the behavior of a microsensor using the strategy discussed above, by solving the governing convection/reaction/diffusion equations numerically using Matlab and COMSOL, while imposing the above boundary conditions and initial condition $c_0 = 1$. Using the parameters given in the main text, we calculate $\mathrm{Pe_H} = 1.67$ x 10^5, $\lambda = 0.5$, $\mathrm{Da}^* = 332$, $\tilde{c} = 10^{-5}$, and $\epsilon^* = 3$ x 10^{-8}.

A straightforward extension of this approach to simulate the nanosensor would be computationally too expensive – the tremendous mesh refinement required around a sensor that is $\lambda = 10^{-4}$ smaller than the channel height would simply require too many mesh points to resolve everything sufficiently. We thus introduce a modified problem formulation and code. As discussed in the text, the nanowire system under study has $\mathrm{Pe_H} \sim 10^5$, and $\lambda = 10^{-4}$, giving a depletion zone that is small compared with the channel but large compared with the sensor. The depletion zone is this 'extended' compared with the sensor geometry, yet never 'feels' the top of the channel. Rather than simulate the full channel, therefore, we simulate a region that is large enough to contain the depletion zone, yet still much smaller than the full channel. In this computational zone, the fluid flow velocity looks like simple shear flow $\vec{u'}(y') = \dot{\gamma}\ y'$ with shear rate $\dot{\gamma}$. Note that the channel height is no longer relevant in this simulation, so we non-dimensionalize y instead with the sensor length L, obtaining

$$\frac{\partial c}{\partial t} = \frac{\partial^2 c}{\partial x^2} + \frac{\partial^2 c}{\partial y^2} - \mathrm{Pe_s} y \frac{\partial c}{\partial x}, \tag{37}$$

where $\mathrm{Pe_s} = 6\lambda^2\ \mathrm{Pe_H}$ as above.

The Langmuir binding equation and the reaction/flux boundary condition for the convection-diffusion equation must also be non-dimensionalized with $y = y'/L$ to obtain

$$\frac{\partial b}{\partial t} = \epsilon^\dagger \mathrm{Da}^\dagger \left[c|_{y=0}(1-b) - \frac{b}{\tilde{c}} \right], \tag{38}$$

where $\mathrm{Da}^\dagger = k_{\mathrm{on}} b_{\max} L/D$ and $\epsilon^\dagger = c_0 L/b_{\max}$. Note that $\mathrm{Da}^\dagger$ and $\epsilon^\dagger$ differ from Da^* and ϵ^* by a factor of λ. Another modification follows from the observation that $c|_{y=0}(1-b) \sim \mathcal{O}(1)$ and $\frac{1}{\tilde{c}} b \sim \mathcal{O}(10^5)$, yet at steady-state the two balance. The errors introduced by computational round-off and numerical imprecision can cause trouble in accurately tracking the evolution of terms of such widely-varying sizes. Instead, we non-dimensionalize the bound concentration b' by the equilibrium amount b_{eq}, a new scaling, $b^\dagger = b'/b_{\mathrm{eq}}$, where b_{eq} is the surface concentration of bound analyte

at equilibrium. Doing so, we obtain

$$\frac{\partial b^\dagger}{\partial t} = \frac{\epsilon^\dagger \mathrm{Da}^\dagger}{\tilde{c}}[c|_{y=0}(\beta - b^\dagger)\tilde{c} - b^\dagger], \tag{39}$$

where $\beta = b_{\max}/b_{\mathrm{eq}}$. The two terms in brackets are now both $\mathcal{O}(1)$ as desired.

II. PHASE DIAGRAM FOR MASS TRANSPORT

We discuss briefly the location of the boundaries in Fig. 3(A) in the main text, which depicts the qualitatively different mass transport behaviors that occur for different sensor length $\lambda = L/H$ and channel Peclet number $\mathrm{Pe_H}$. We assume throughout this section that the channel and sensor have the same width, $W_c = W_s \equiv W$. We treat the sensor as a perfect collector, such that all target molecules that diffusively encounter it are collected. In this fashion, the following analysis (as well as Fig. 3(A) more generally) represent the mass transport-limited regime, which can be modified or incorporated (as we did in the main text) to treat the full convection-diffusion-reaction system.

We begin with Region II, which involves a very thin depletion zone, whose thickness $\delta \sim L\mathrm{Pe_s}^{-1/3}$ must be small compared with the sensor. For this limit to hold, the sensor (or shear) Peclet $\mathrm{Pe_s}$ must itself be large, which requires

$$\mathrm{Pe_s} \sim \lambda^2 \mathrm{Pe_H} \gg 1, \text{ or } \ln \mathrm{Pe_H} \gg -2\ln\lambda. \tag{40}$$

Secondly, the depletion zone must be small compared to the channel height – which becomes relevant for 'long' sensors ($\lambda \gg 1$):

$$\delta \sim \mathrm{Pe_s}^{-1/3} L \ll H,, \text{ or } \lambda^{-2/3}\mathrm{Pe_H}^{-1/3} \ll \lambda^{-1}, \tag{41}$$

giving

$$\mathrm{Pe_H} \gg \lambda. \tag{42}$$

Thus the boundaries of Region II are formed by Equations (40) and (42).

We turn now to Region III, wherein the depletion layer is thin compared with the channel,

$$\mathrm{Pe_H} \gg 1, \tag{43}$$

but is much thicker than the sensor itself,

$$\mathrm{Pe_s} \sim \lambda^2 \mathrm{Pe_H} \ll 1, \tag{44}$$

(i.e. it only occurs for short sensors $\lambda \ll 1$). The above conditions put region II to the left of (40); however, one expects to eventually cross into 'full collection' of all analyte molecules if the flow rate is slow enough.

The 'full collection' regime (region I) for large sensors ($\lambda > 1$) lies to the left of (42): if the flow is slow enough that the depletion zone above the sensor spans the channel height H (even though $\mathrm{Pe_s}$ may be large), then almost all target molecules will be captured. Its location for small sensors, on the other hand, is less trivial. The channel Peclet number $\mathrm{Pe_H}$ must be low – to determine how small $\mathrm{Pe_H}$ must be, we note that there are three qualitatively different regions of transport: (a) convective transport far upstream with flux,

$$J = Qc_0, \tag{45}$$

(b) a 'one-dimensional' depletion zone that extends from an upstream distance δ (where $c = c_0$) to a distance of order H from the sensor (where concentration is an as-yet unknown value c^*), giving a one-dimensional diffusive flux

$$J \sim DW(c_0 - c^*)/\delta \sim D\mathrm{Pe_H}W(c_0 - c^*), \tag{46}$$

and (c) a two-dimensional, approximately radial diffusive flux onto the sensor, with concentration profile

$$c(r) \sim c^* \frac{\ln r/L_s}{\ln H/L} = c^* \frac{\ln r/L}{\ln(1/\lambda)}, \tag{47}$$

which goes from the (unknown) concentration c^* at $r = H$ and to zero (perfect collection) at $r = L_s$. The total diffusive flux here is

$$J_D \sim DW \frac{c^*}{\ln(1/\lambda)}. \tag{48}$$

For full collection, all three of these fluxes must balance, which determines δ and c^*. In particular, a boundary for perfect collection is found by equating the 'upstream flux' (a) and the radial diffusive flux near the sensor (c), requiring

$$DW\frac{c^*}{\ln(1/\lambda)} \sim Qc_0 \rightarrow \frac{c^*}{c_0} \sim \mathrm{Pe_H}\ln(1/\lambda). \tag{49}$$

Since the concentration c^* is necessarily smaller than c_0, the upper flow rate (or $\mathrm{Pe_H}$) for full collection is given by

$$\mathrm{Pe_H} \ll \frac{1}{\ln(1/\lambda)}, \tag{50}$$

which appears in fig. 3(A). The slower the flow ($\mathrm{Pe_H}$), the farther the depletion zone extends upstream, and therefore the smaller c^*.

One final regime – labelled IV in fig. 3(A) in the main text – has not, to our knowledge, been investigated in the literature thus far. It exists for small sensors, and lies between the 'full collection' and low $\mathrm{Pe_s}$ diffusion in shear flow. Depletion zones in region IV are bigger than the sensor, but are also comparable to or larger than the channel height.